

Unsupervised Oil Slick Detection by SAR Imagery using Kernel Expansion

Grégoire MERCIER* and Fanny GIRARD-ARDHUIN†‡

*GET/ENST Bretagne, dpt ITI,
TAMCIC, team TIME, CNRS UMR 2872,
Technopôle Brest-Iroise, CS 83818,
F-29 238 Brest Cedex, France.

†IFREMER DOPS/LOS,
Technopôle Brest-Iroise, BP 70,
F-29 280 Plouzané, France.

‡CNES,
2 place Maurice Quentin,
F-75 001 Paris, France.

Abstract—Spaceborne Synthetic Aperture Radar is well adapted to detect ocean pollution independently from daily or weather condition. In fact, oil slicks have specific impact on ocean wave spectra. Initial wave spectra may be characterized by three kinds of waves, big, medium and small, which correspond physically to gravity and gravity-capillary waves. The increase of viscosity due to the presence of oil damps gravity-capillary waves. This induces a damping of the backscattering to the sensor, but also a damping of the energy of the wave spectra. Thus, local segmentation of wave spectra may be achieved by the segmentation of a multiscale decomposition of the original SAR image.

In this work, an unsupervised oil slick detection is proposed by using kernel-based novelty detection into the wavelet decomposition of a SAR image. It performs accurate detection with no consideration to signal stationarity nor to the presence of strong backscatters (such as ship).

The algorithm has been applied on ENVISAT ASAR images. It yields accurate segmentation results, even for small slicks, with a very limited number of false alarms.

I. INTRODUCTION

The oceanic sea surface is complex and often governed by non-linear dynamic systems. Surface waves, that are found in the ocean, range from the millimeter scale to hundreds of meters. By considering an infinite sea surface, the wind induces capillary waves by friction. Capillary waves cannot propagate and they vanish with the wind. But they transfer their energy to waves with a longer wavelength until they reach an equilibrium that depends on the wind. In addition, gravity waves transfer their energy to gravity-capillary waves. Several models have been proposed to characterize the sea surface spectrum with an accuracy that depends on the wavelength bandwidth. Those models integrate the wind, but also the current, atmospheric pressure and so on. An interesting comparison of some models may be found in [1] in the context of SAR imagery. On the one hand, capillary waves are generated by friction, and more specifically by friction velocity, related by wind speed and surface properties, which die down when the friction decreases. On the other, gravity waves are generated indirectly by sea spectrum energy spreading and propagating over long distances far from their origins.

In fact, backscattering phenomena are directed by gravity-capillary waves (due to the wavelength of electromagnetic waves) while typical SAR systems are sensitive to gravity waves (due to their resolution).

A. Sea surface observation with SAR data

Radar electromagnetic waves are backscattered by the sea surface. The simplest model that describes this backscattering process is the Bragg resonance effect that links the sea surface and electromagnetic wavelengths. According to this model, the sea surface waves of wavenumber $\kappa_{\text{sea}} = 2\kappa_{\text{SAR}} \sin \theta$ contribute to the scattering process (κ_{SAR} being the wavenumber of the electromagnetic wave and θ the incidence angle).

More precisely, most SAR sensors that are used on civil satellites use the C band (*i.e.* a wavelength of about 5.6 cm). By considering incidence angles from 15 to 45° according to the sensors and their acquisition modes, gravity-capillary waves of wavelengths from 4 to 14 cm intervene in the scattering process.

Nevertheless, SAR image resolution is much larger than the wavelength and the sensor is sensitive to large scale oceanographic phenomena. In fact, the Bragg mechanism considers waves of one wavelength only [2] while it is necessary to consider a bandwidth or, even better, the overall wave spectrum. Moreover, wave motion induces specific modulation on the wave spectrum acquired by the SAR sensor. Hence, surface roughness induced by short waves is modulated by longer waves allowing SAR imagery to characterize “indirectly” oceanophysical phenomena such as swell, internal waves, coastal bathymetry or oil slicks.

B. Usual strategy for oil spill detection

A viscous area is seen smoother than a clean sea surface since small wave generation and propagation is stopped by the viscosity of a slick. From the SAR sensor point of view, a slick is characterized by a lack of backscattered energy and then restituted through a dark area [3]. According to the Bragg phenomenon, the backscattering process is mostly due to surface roughness.

That is why many slick detection algorithms are based on a thresholding technique [4–6]. Nevertheless, this process is not efficient when:

- the wind is increasing (basically over 10-14 m/s);
- the sea state is different (more precisely its wave spectrum shape);
- viscoelastic oil properties are different (different kinds of oil but also their degradation);
- possible bad-detection with look-alikes (*e.g.* weak wind area, upwelling, phytoplankton, algae, etc.).

Moreover, a radiometric point of view shows some limitations since wave slopes that are not oriented to the sensor are restituted with a lower radiometry that may be confused with small slicks. That is why most slick detection strategies include a post-processing stage to remove small slicks through geometrical, morphological or contextual criteria [7–9].

C. Multiscale strategy

A priori, the proposed multiscale strategy that is implemented to detect oil slicks may be justified by several concepts mentioned above:

- the SAR sensor is only sensitive to surface roughness (at a centimeter scale) which is modulated by larger scale phenomena that induce shades of texture;
- the increase of viscosity, due to the presence of an oil slick on the sea surface, affects the sea surface wave spectrum shape;
- oil slicks induce dark areas on the SAR images under certain conditions, such as a limited wind (*i.e.* under 10-14 m/s).

The multiscale strategy has been already proposed in previous studies [10, 11]. In [10], the methodology has been developed by using Markov chain that is sensitive to the scene stationarity. But a slick is rarely statistically representative. In [11], oil slick detection is performed by using Support Vector Machines into a Supervised classification process. It is understood from supervised technique that end user has found a Region of Interest (ROI) that defines non polluted sea *and* a ROI dedicated to oil slick. It is some time difficult to define those ROIs in an operational context. Also, ROIs may not be representative to the slicks that may be found into the scene (large or thin slicks, heavy, volatil or degraded oil). The way unsupervised technique is developed here is to recognise the sea surface from a training set. Every thing else will be considered as oil. In order to minimize the false alarms, the feature space is defined carefully by considering the multiscale representation and also the textural information deduced from the wavelet coefficients.

Since the multiscale representation is the same as the one presented in [10], we just remind that the initial SAR image is represented with its details at different scales [12] by:

$$I \longrightarrow \begin{cases} I_L^{\text{low}} & = I(x, y) * \theta(2^{-(L-1)}x, 2^{-(L-1)}y) \\ I_\ell^{\text{hori}} & = I(x, y) * \psi^{\text{hori}}(2^{-\ell}x, 2^{-\ell}y) \\ I_\ell^{\text{vert}} & = I(x, y) * \psi^{\text{vert}}(2^{-\ell}x, 2^{-\ell}y). \end{cases} \quad (1)$$

In section II, abnormal detection is defined through Support Vectors. Section III focuses on kernel definition to perform an abnormal detection in the way of slick detection. Section IV shows two typical examples from ENVISAT SAR data. Section V concludes.

II. SUPPORT VECTORS FOR ABNORMAL DETECTION

Lets consider an observation x issued from a SAR acquisition and transformed into a vector \mathbf{x} according to eq. (1). For oil slick detection, we propose to solve the following problem:

$$\begin{aligned} \mathcal{H}_{\text{sea}} &: \mathbf{x} \sim p_{\text{sea}} \\ \mathcal{H}_{\text{-sea}} &: \mathbf{x} \not\sim p_{\text{sea}} \end{aligned}$$

that is to say: if \mathbf{x} is distributed according to the probability density function (pdf) that characterizes the sea surface, it may be considered as representative to the sea surface (hypothesis \mathcal{H}_{sea}). On the contrary, if \mathbf{x} is not distributed according to p_{sea} it cannot be considered as representative to the sea surface (hypothesis $\mathcal{H}_{\text{-sea}}$).

A general solution of this problem consist in building a decision function $f(\cdot)$ where \mathcal{H}_{sea} is decided if $f(\cdot) > 0$:

$$f(\mathbf{x}) \underset{\mathcal{H}_{\text{-sea}}}{\overset{\mathcal{H}_{\text{sea}}}{\geq}} 0. \quad (2)$$

In that problem, the pdf p_{sea} is not known and has to be estimated with a training set. Kernel expansion has been chosen since this technique does not require the knowledge of the statistical model p_{sea} and provides computationally efficient decision function. This technique is known as *Support Vector Novelty Detection* [13].

In the linear case (as shown on Fig. 1-a), the decision function is to be built with

$$\begin{aligned} f(\mathbf{x}) &= \langle \mathbf{x}, \mathbf{w} \rangle - \rho \\ &= \sum_{i=1}^m \alpha_i \langle \mathbf{x}, \mathbf{x}_i \rangle - \rho \end{aligned} \quad (3)$$

where $\{\mathbf{x}_1, \mathbf{x}_2, \dots, \mathbf{x}_m\}$ is the m -sample training set. If the training set is separable, then there exists a unique supporting hyperplane with the properties that:

- 1) it separates all the data from the origin,

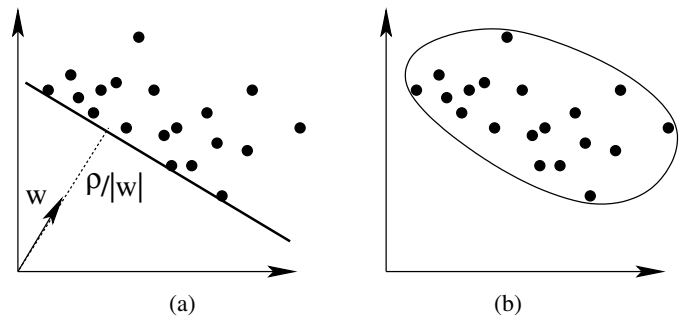


Fig. 1. A separable data set, (a) with the unique supporting hyperplane separating data from the origin with maximum margin, (b) with a non-linear characterization.

- 2) its distance to the origin is maximal among all such hyperplanes.

The supporting hyperplane is given by:

$$\underset{\mathbf{w}}{\text{minimize}} \frac{1}{2} \|\mathbf{w}\|^2 \quad \text{subject to} \quad \langle \mathbf{w}, \mathbf{x}_i \rangle \geq \rho,$$

$$\forall i \in \{1, 2, \dots, m\}.$$

III. KERNEL-BASED ABNORMAL DETECTION

Let Φ be the feature map that transforms initial SAR observation into a feature space (\mathcal{H}) where oil slick signatures are becoming highly contrasted. The initial dot product is transformed into a kernel evaluation:

$$K(\mathbf{x}, \mathbf{x}') = \langle \Phi(\mathbf{x}), \Phi(\mathbf{x}') \rangle.$$

Then, $\mathbf{w} = \sum_i \alpha_i \Phi(\mathbf{x}_i)$. The decision function becomes

$$f(\mathbf{x}) = \sum_{i=1}^m \alpha_i K(\mathbf{x}_i, \mathbf{x}) - \rho \quad (4)$$

that is given by the dual problem:

$$\underset{\mathbf{w} \in \mathcal{H}}{\text{minimize}} \frac{1}{2} \sum_{i,j \in \{1, \dots, m\}} \alpha_i \alpha_j K(\mathbf{x}_i, \mathbf{x}_j) \quad (5)$$

$$\text{subject to } 0 \leq \alpha_i \leq \frac{1}{\nu m} \quad \text{and} \quad \sum_{i=1}^m \alpha_i = 1.$$

Here, $\nu \in]0, 1]$ is introduced in close analogy to the ν -SV classification algorithm. If ν tends to 0, the upper bounds on the Lagrange multipliers tend to infinity and the constraint of eq. (5) vanishes and we are facing a *hard margin* problem.

A. Usual kernels

For oil slick segmentation, we observed that polynomial, eq. (6), or sigmoid kernels, eq. (7), were the more satisfactory since they minimize the number of false alarms:

$$K_{\text{Polynomial}}(\mathbf{x}, \mathbf{s}_i) = (\langle \mathbf{x}, \mathbf{s}_i \rangle + 1)^p, \quad (6)$$

$$K_{\text{Sigmoid}}(\mathbf{x}, \mathbf{s}_i) = \tanh(\langle \mathbf{x}, \mathbf{s}_i \rangle + 1). \quad (7)$$

Those kernels are based on the classical dot product and \mathbf{x} tends to 0 (*i.e.* a lower radiometry and surface roughness) into the slicks.

B. Texture kernels

It is of interest to consider not only pointwise observations through vector-to-vector comparisons but also local neighbourhoods to perform the local characterization of the sea surface wave spectra. A texture-based kernel has been developed in order to act as a contrast measurement of local texture on each component of the vectors.

Let's consider the neighbourhood of each component of vectors \mathbf{x} and \mathbf{y} . In this study, each component of vectors for the SVM approach are wavelet coefficients. Furthermore the neighbourhood concept is to be understood as a spatial neighbourhood on the image (on the sea surface) and not as a Voronoï cell in the n or the \mathcal{H} space.

For accuracy of local parameter estimation, local probability density functions (pdf) have been chosen to follow the Gaussian law that is supposed to be independent from a component to another. Distributions are compared through the Bhattacharyya distance.

Thus, the texture kernel may be defined, as a RBF kernel, as:

$$K(\mathbf{x}, \mathbf{y}) = e^{-(1-\mathcal{B}(p_{\mathbf{x}}, p_{\mathbf{y}}))}, \quad (8)$$

$$\text{with} \quad \mathcal{B}(p_{\mathbf{x}}, p_{\mathbf{y}}) = \prod_{\ell=0}^{L-1} \int \sqrt{p_{x_\ell}(u) p_{y_\ell}(u)} du.$$

Since $\mathcal{B}(p_{\mathbf{x}}, p_{\mathbf{y}}) \in [0, 1]$, kernel of eq. (8) satisfy the Mercer's conditions.

C. Mixture of kernels

It is of interest to consider the backscattering process but also its local shape. Then, linear mixture of kernels can fit the dual point of view: similarity according to the dot product and also similarity according to the texture. Mixture of kernels may be defined as [14]:

$$K(\mathbf{x}, \mathbf{x}_i) = \mu K_a(\mathbf{x}, \mathbf{x}_i) + (1 - \mu) K_b(\mathbf{x}, \mathbf{x}_i), \quad (9)$$

where $K_a(\cdot, \cdot)$ and $K_b(\cdot, \cdot)$ are two kernels. Since $K_a(\cdot, \cdot)$ and $K_b(\cdot, \cdot)$ satisfy Mercer's conditions, all linear combinations are eligible for kernels.

IV. APPLICATIONS

Let's summarize the procedure for oil slick detection:

- 1) SAR image I is composed into a multiscale representation that yields a vector with $2L + 1$ components: $(I^{\text{low}}, I_{L-1}^{\text{hori}}, I_{L-1}^{\text{vert}}, \dots, I_0^{\text{hori}}, I_0^{\text{vert}})^t$, according to eq. (1).
- 2) A ROI is defined from a non-polluted sea area to the SVM design as eq. (5).
- 3) The overall classification is performed by the kernel expansion of eq. (4).

A. Oil Slick

A typical example has been chosen during the Prestige's wreck on November 2002, near the Spanish coasts. The Envisat ASAR image has been acquired on November 17 (10h45 UTC, orbit 3741, pol VV, Wide Swath mode, pixel size 75×75 m) that is 4 days after the accident and 2 days before it sunk. Wreckage can be seen as strong backscatters on the bottom left of image (a) on Fig. 2. The slick by itself is easy to detect (since meteorological conditions, shown by QuickScat observations, proved there is enough wind — 7 to 10 ms^{-1} — to exclude a detection of a natural film). Nevertheless some dark areas (due to an atmospheric perturbation) often induce false alarms.

Kernel expansion has been trained in a small area delimited by the white square on Fig. 2-a. Decision of eq. (2) has been applied and yield the results shown on Fig. 2-b.

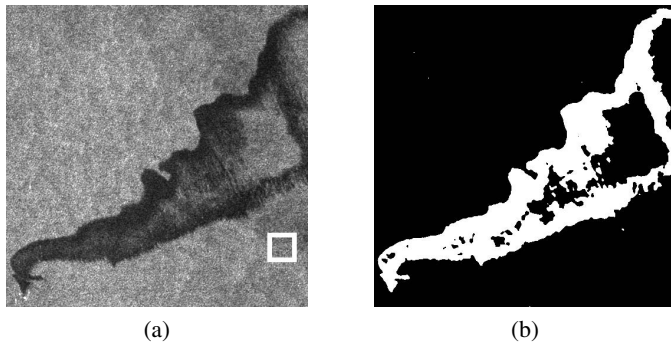


Fig. 2. Detection results on ENVISAT ASAR image, November 17, 2002. (a) initial image with the ROI used to define the decision function (3550 pixels). (b) detection results.

B. Oil spill

An other example has been selected from an Envisat acquisition of the same area (South of Galicia) but not connected to the Prestige's wreck. This image of Fig. 3-a acquired on January 6th, 2003 (22h30 UTC, orbit 4464, pol VV, Wide Swath mode, pixel size 75×75 m) shows a 30 km long thin linear oil spill that is difficult to detect due to the swell (h_s estimated to 5 m) but the wind (5 to 12 ms^{-1} according wind estimation from the SAR image itself and QuickScat data) is strong enough to ensure a spill detection. The 6308 pixel ROI include dark area induced by atmospheric conditions. The spill detection still shows false alarms but the detection itself remains accurate. Also, Distance map to the hyperplane (values of eq. (4) shown on Fig. 3-c) can be used to connect the linear spill. Moreover, the distance map shows that ships (that appear in dark on Fig. 3-c) are located to the opposite side of the feature space \mathcal{H} from the spill. It confirms the good choice of the kernel.

V. CONCLUSION

An unsupervised oil slick detection technique is proposed by using Support Vector Machines into a wavelet decomposition of a SAR image. A specific kernel is developed to perform accurate segmentation of local sea surface wave spectrum by using both radiometric and texture information.

Instead of previous studies, such as [10, 11], this technique is efficient in an operational context and proved to be a relevant strategy to detect oil slicks as abnormal situations of the sea surface roughness and radiometry.

ACKNOWLEDGMENT

This work has been funded by the RITMER program of French Ministry of Research under the name DetecSuiv, conducted with SAS ActiMar.

REFERENCES

[1] T. Elfouhaily and B. Chapron, "A comparison of wind wave spectra used in ocean remote sensing modeling," in *Proc. of the IEEE IGARSS'96*, vol. 1, Lincoln, NE (USA), 27-31 May 1996, pp. 606-608.
 [2] J. W. Wright, "A new model for sea clutter," *IEEE Trans. Antennas Propagat.*, vol. 16, pp. 217-223, 1968.

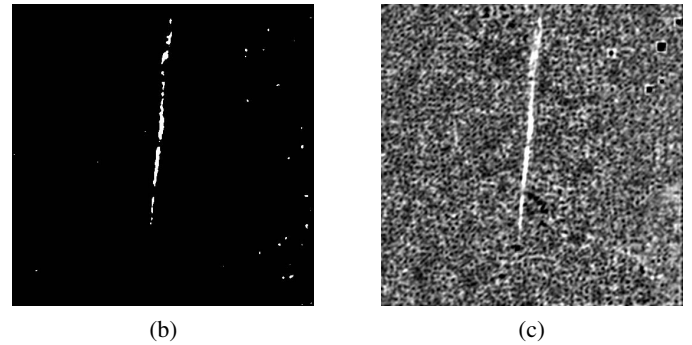
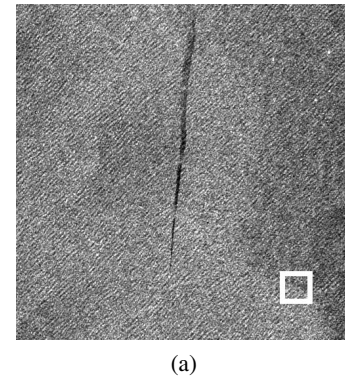


Fig. 3. Detection results on ENVISAT ASAR image, January 6th, 2003. (a) initial image with the ROI used to define the decision function (6308 pixels). (b) detection results, (c) distance to hyperplane.

[3] M. Gade, W. Alpers, H. Hühnerfuss, V. Wisman, and P. Lange, "On the reduction of the radar backscatter by oceanic surface films: Scatterometer measurements and their theoretical interpretation," *Remote Sensing of Environment*, vol. 66, pp. 52-70, 1998.
 [4] M. Gade, J. Scholz, and C. von Viebahn, "On the detectability of marine oil pollution in European marginal waters by means of ERS SAR imagery," in *Proc. of the IEEE IGARSS'00*, vol. 6, Honolulu, HI (USA), 24-28 July 2000, pp. 2510-2512.
 [5] P. Lombardo, D. Conte, and A. Morelli, "Comparison of optimised processors for the detection and segmentation of oil slicks with polarimetric SAR images," in *Proc. of the IEEE IGARSS'00*, vol. 7, Honolulu, HI (USA), 24-28 July 2000, pp. 2963-2965.
 [6] Bjerde, A. H. S. Solberg, and R. Solberg, "Oil spill detection in SAR imagery," in *Proc. of the IEEE IGARSS'93*, vol. 3, Tokyo, Japan, 18-21 August 1993, pp. 943-945.
 [7] A. H. S. Solberg, G. Storvik, R. Solberg, and E. Volden, "Automatic detection of oil spills in ERS SAR images," *IEEE Trans. Geosci. Remote Sensing*, vol. 37, pp. 1916-1924, July 1999.
 [8] H. Espedal, "Detection of oil spill and natural film in the marine environment by spaceborne SAR," in *Proc. of the IEEE IGARSS'99*, vol. 3, Hamburg, Germany, 28 June, 2 July 1999, pp. 1478-1480.
 [9] M. Bertacca, F. Berizzi, E. Dalle Mese, and A. Capria, "A FARIMA-based analysis for wind falls and oil slicks discrimination in sea SAR imagery," in *Proc. of the IEEE IGARSS'04*, Anchorage, AK (USA), 20-24 Sept 2004.
 [10] G. Mercier, S. Derrode, W. Pieczynski, J.-M. Le Caillec, and R. Garello, "Multiscale oil slick segmentation with markov chain model," in *Proc. of the IEEE IGARSS'03*, Toulouse, France, July 21-25, 2003.
 [11] G. Mercier and F. Girard-Ardhuin, "Oil slick detection by sar imagery using support vector machines," in *Proc. of the IEEE Oceans'05 Europe*, Brest, France, June 20-23, 2005.
 [12] S. Mallat, *A Wavelet Tour of Signal Processing*. Academic Press, 1998.
 [13] V. N. Vapnick, *Statistical Learning Theory*. John Wiley and Sons Inc., 1998.
 [14] G. Smits and E. Jordaen, "Improved SVM regression using mixtures of kernels," in *IJCNN*, 2002.